

Classical and integrated multicomponent geothermometry at the Tengchong geothermal field, Southwestern China

Tianfu Xu¹ · Zhaoyun Hou¹ · Xiaofeng Jia² · Nicolas Spycher³ · Zhenjiao Jiang¹ · Bo Feng¹ · Jin Na¹ · Yilong Yuan¹

Received: 29 May 2016 / Accepted: 28 November 2016 / Published online: 17 December 2016
© Springer-Verlag Berlin Heidelberg 2016

Abstract To reconstruct deep fluid chemical composition and increase the confidence in estimated reservoir temperatures, a more integral geothermometry method was compared to other classical geothermometers. Here, we apply the integrated multicomponent geothermometry (IMG) method using the GeoT code to estimate reservoir temperatures at the Tengchong geothermal field in Southwestern China. Results show reservoir temperatures calculated using the quartz geothermometer are closest to those estimated with the IMG method. The concentrations of Al and Mg, as well as selected minerals for geothermometry computations, are key factors for successfully using the IMG. Using the IMG method together with classical geothermometers can significantly increase confidence in reservoir temperature estimations. The methods presented and simulation program used here may be useful for analysis of other geothermal fields under similar conditions.

Keywords Reservoir temperature · Quartz geothermometer · Integrated multicomponent geothermometry · Numerical optimization · Tengchong geothermal field

Introduction

Chemical geothermometers have been applied to estimate geothermal reservoir temperature for decades, by analyzing correlations between fluid chemical composition and temperature. The most commonly applied chemical geothermometers are known as “classical” or “traditional” geothermometers, such as silica (Fournier and Potter 1982), Na–K (Fournier 1979; Giggenbach 1988), Na–K–Ca (Fournier and Truesdell 1973) and K–Mg geothermometers (Giggenbach 1988). These geothermometers have been widely and mostly successfully applied to estimate deep reservoir temperatures. However, the results of these geothermometers can be affected by processes such as degassing, mixing/dilution and reactions with various minerals when deep fluids rise to the ground surface.

These classical geothermometers each have their own advantages and differing ranges of applicable conditions. For example, based on the equilibrium between albite and K-feldspar, the Na–K geothermometer is generally considered to represent the deep reservoir temperature, as the concentration ratio is unaffected by dilution. However, in reservoirs with low temperatures, the Na/K ratio may depend on other minerals, such as montmorillonite, in which case this geothermometer would give incorrect results. The K–Mg geothermometer is semiempirical, based on the equilibrium of muscovite, clinocllore and K-feldspar. Because the dissolved concentration of Mg in deep fluids at equilibrium with these minerals is typically

This article is part of a Topical Collection in Environmental Earth Sciences on ‘Subsurface Energy storage II’, guest edited by Zhonghe Pang, Yanlong Kong, Haibing Shao, and Olaf Kolditz.

✉ Bo Feng
fengbo234@126.com

¹ Key Lab of Groundwater Resources and Environment, Ministry of Education, Jilin University, Changchun 130021, China

² Center for Hydrogeology and Environmental Geology Survey, China Geological Survey, Baoding 071051, China

³ Earth Sciences Division, Lawrence Berkeley National Laboratory, Berkeley, CA 94720, USA

extremely low (often below the detection limit), the original equilibrium K/Mg ratio is quite sensitive to re-equilibration when deep fluid ascends to the ground surface (e.g., Peiffer et al. 2014). Therefore, the K–Mg geothermometer is often used for shallow geothermal reservoirs or used to represent “last” equilibration temperatures. Because the Na–K–Ca geothermometer is very sensitive to CO₂ concentration and the consequent precipitation/dissolution of calcite, it is often best applied to Ca-rich waters.

The multicomponent geothermometer is based on the theoretical thermodynamic equilibration of multiple minerals with a geothermal fluid, computed from the clustering of mineral saturation indices ($\log(Q/K)$ curves) near zero at the equilibration temperature, using a variety of dissolved components (Reed and Spycher 1984; Pang and Reed 1998). Compared with classical geothermometers, multicomponent geothermometry has the advantage of complete fluid analyses and numerical calculations that have a thermodynamic basis, rather than the solubility of a few minerals or (semi-)empirical correlations. Also, it is technically applicable to any geochemical system. However, multicomponent geothermometry requires detailed aqueous chemistry and mineralogical data, so it is less frequently applied than classical geothermometers (Ding 2013). Moreover, when determining the clustering of computed $\log(Q/K)$ curves, using this method may present judgmental errors because it relies on visual inspection.

In view of the above problems, integrated multicomponent geothermometry (IMG) following the approach presented by Spycher et al. (2014) and Peiffer et al. (2014) was applied to reconstruct the chemical composition of deep fluids and estimate the temperature of the Tengchong geothermal reservoir. In addition, the influences of gas loss, mixing/dilution, different mineral assemblages and the concentration of Al and Mg on estimating the geothermal temperature were also investigated.

Geological setting

The Tengchong volcanic region in Yunnan Province is located at the edge of the Eurasian plate and the Indian plate. In this area, Late Cenozoic volcanic activity and modern fault structure activity occur frequently. Large quantities of granite, which are rich in radioactive elements, provide an abundant heat source for the geothermal region (Tong and Zhang 1989).

The Rehai geothermal field is one of the most active fields in the area. It has a total area of 10 km² and is located in the southwest region of Tengchong County, in the north central zone of the Tengchong–Longchuan hydrothermal activity region. It includes a large active hydrothermal area with various kinds of geothermal springs (Fig. 1a, b). The

Rehai geothermal field is closely related to recent volcanic activity, and the fault structure is helpful for fluid and heat conduction (Figs. 1c, 2). The hydrothermal activities mainly occur at the intersection part of three north–south trending faults (F5, F6 and F7, respectively) and an East–west trending fault (F38). This geothermal field contains not only hot springs but also boiling springs. There are some hot springs with elevated temperatures above 80 °C, but lower than the local boiling point, such as Laogunguo, Dagunguo, Xiaogunguo, Yanjingquan, Diretiyanqu, Zhenzhuquan, Huaitaijing and Gumingquan. Other hot springs have moderate temperatures above 25 °C but lower than 80 °C, such as Dabaiyan, Xianrenzaotang, Zhongxiaosi, Shizitang and Yangjiapo. The remaining springs are steaming ground and fumaroles, including Zhonghuangdian, Huangguoqing and Shapo-Songmuqing (Guo 2013).

Chemical composition of hot springs

Spring water sample data used in this study came from the analysis of samples reported by Liu et al. (2014), who collected a total of 13 water samples near the Zaochang River (Fig. 1c). The chemical compositions of these hot spring samples are listed in Table 1.

As can be seen from Table 1, the dominant cations in most hot spring samples are Na⁺ and K⁺, while the concentrations of Ca²⁺ and Mg²⁺ are very low. In most samples, the main anions are Cl[−] and HCO₃[−], while SO₄^{2−} is the main anion only in RH03 and RH06. There are three dominant anions in RH05, which are CO₃^{2−}, Cl[−] and HCO₃[−]. The pH value in RH06 is 2.6, whereas the rest of samples exhibit a weak acidic or weak alkaline character (pH 6.4–9.2). Among all water samples, RH03 and RH06 are most different, with high concentrations of SO₄^{2−} and low concentrations of Na⁺, Cl[−] and HCO₃[−]. Because the local shallow groundwater contains low concentrations of Na⁺, Cl[−] and HCO₃[−], we speculate that degassing of H₂S and SO₂, followed by mixing with shallow groundwater, generated acid solutions rich in SO₄^{2−} but diluted with respect to Na⁺, Cl[−] and HCO₃[−] when the deep fluid ascended to the ground surface.

More detailed data about the relationship between Na⁺ and Cl[−] in these spring waters are shown in Fig. 3 (Shangguan 2000), which include 19 hot springs and two cold springs. Figure 3 shows that all the springs fall on the same Na/Cl trend, even though these springs originate from different faults (Fig. 1c). The Na/Cl ratio appears to be controlled only by mixing with shallow groundwater, because the shallow groundwater has very low concentrations of Na⁺ and Cl[−]. This infers that the hot springs in this geothermal field may share a common heat source, a hypothesis which we further test in our investigation of deep reservoir temperatures.

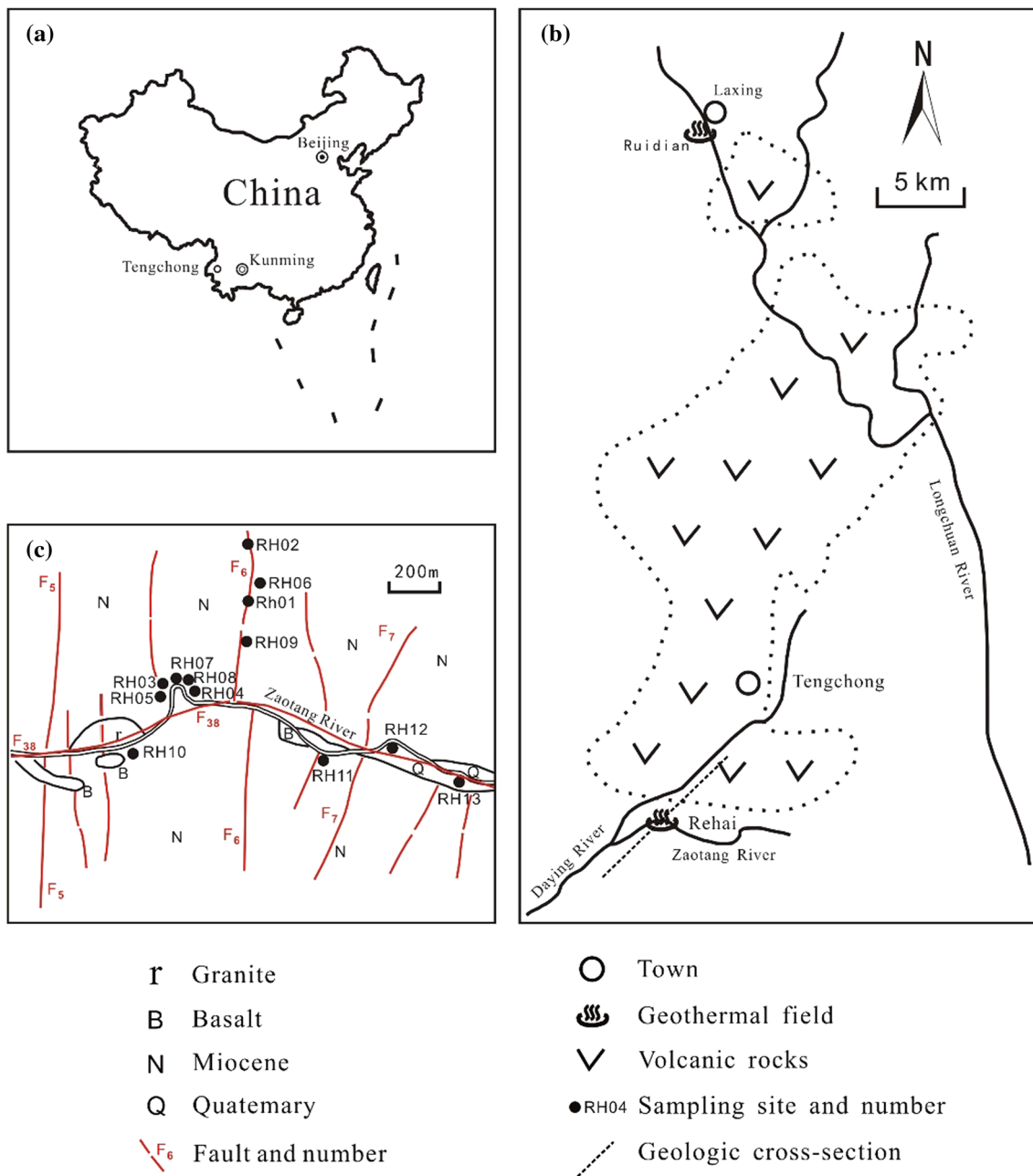


Fig. 1 a, b Location of the Rehai geothermal field, c sampling sites in the Rehai geothermal field (Liu et al. 2014)

Integrated multicomponent geothermometry approach

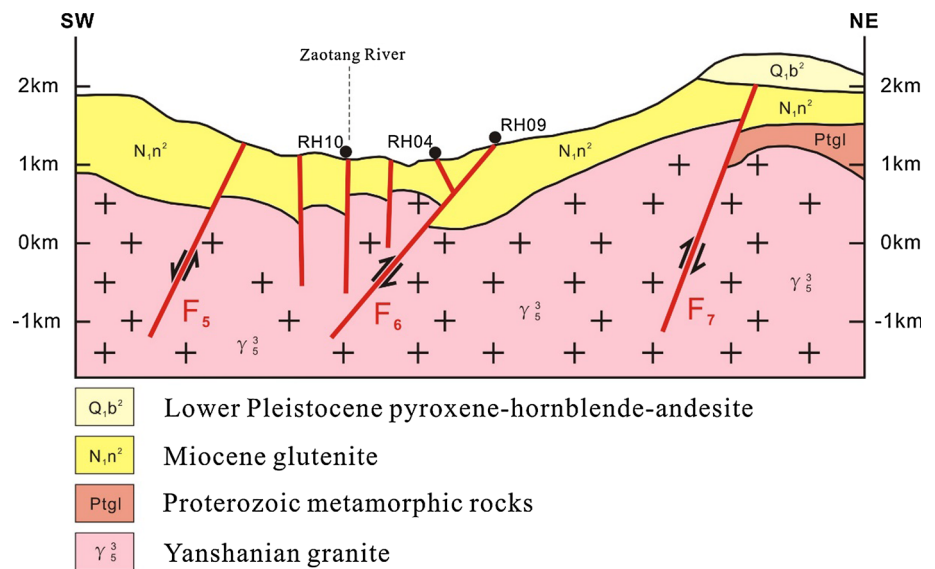
Mineral assemblage and thermodynamic data

A mineral assemblage was selected based on X-ray diffraction analysis by Lin et al. (2014), who reported that the geothermal reservoir rock is granite (Stage of Yan-shan). Quartz, albite, microcline, clinocllore, muscovite, calcite, tremolite, laumontite and montmorillonite-Ca were taken as the main minerals contained in this granite.

The thermodynamic database SOLTHERM.H06 was used in this simulation, which has been satisfactorily applied to simulate many types of hydrothermal systems (Reed and Palandri 2006).

Simulation program

In this study, the geothermometry simulation program GeoT is used (Spycher et al. 2014). Based on complete chemical composition analyses of the fluid, GeoT calculates the saturation indices of minerals ($\log(Q/K)$) over a

Fig. 2 Geologic cross section of the Rehai geothermal field**Table 1** Chemical composition of the major spring waters from the Rehai geothermal field (mg/L)

Sample no.	Location	T (°C)	pH	HCO_3^-	CO_3^{2-}	SO_4^{2-}	Cl^-	F^-	Ca^{2+}	Mg^{2+}	Na^+	K^+	SiO_2	Hydrochemical type
RH01	Dagunguo	96	8.3	1131.9	35.6	35.2	725.0	18.2	1.0	0.0	689.0	123	889.8	Na–Cl– HCO_3
RH02	Laogunguo	91	6.8	561.0	36.0	23.9	325.0	16.6	0.9	0.0	252.0	53.1	360.0	Na– HCO_3 –Cl
RH03	Zhenzhuquan	96	6.4	5.6	0.0	128.2	39.2	1.0	2.3	0.4	67.7	15.9	262.0	Na– SO_4 –Cl
RH04	Gumingquan	96	8.9	759.7	122.3	18.6	651.0	16.1	1.4	0.0	573.2	107	677.0	Na–Cl– HCO_3
RH05	Yanjingquan	94	8.9	499.8	190.5	15.3	413.6	13.8	0.3	0.0	474.5	83.9	678.7	Na–Cl– HCO_3 – CO_3
RH06	Diretiyanqu	88	2.6	0.0	0.0	682.0	5.9	0.3	30.2	1.3	14.8	24.1	316.9	H– SO_4
RH07	Huaitaijingzuo	88	8.4	857.3	40.8	20.1	558.6	13.8	1.5	0.1	538.3	96.8	304.0	Na–Cl– HCO_3
RH08	Huaitaijingyou	88	7.6	628.5	0.0	38.3	454.6	8.1	1.6	0.0	400.4	71.1	491.0	Na–Cl– HCO_3
RH09	Xiaogunguo	82	7.5	982.9	12.9	20.5	174.8	6.3	11.8	1.4	112.2	33.6	260.5	Na– HCO_3 –Cl
RH10	Wumingquan1	49	9.2	517.8	127.3	32.7	344.7	8.3	1.1	0.3	389.3	72	581.2	Na–Cl– HCO_3
RH11	Wumingquan2	66	6.9	665.4	1.1	52.1	279.5	7.9	2.4	0.1	334.2	51.9	330.0	Na– HCO_3 –Cl
RH12	Wumingquan3	90	8.2	615.6	35.1	23.8	279.5	6.6	2.4	0.2	338.7	50.9	350.0	Na– HCO_3 –Cl
RH13	Wumingquan4	70	8.3	701.7	63.0	34.0	361.9	9.0	4.9	0.5	375.4	68.9	280.0	Na– HCO_3 –Cl

range of temperatures (e.g., 25–300 °C). The saturation indices are graphed as a function of temperature, and the clustering of $\log(Q/K)$ curves near a zero value at any specific temperature is inferred to be the reservoir temperature. This computer program combines the multicomponent chemical geothermometry method by Reed and Spycher (1984) and deep fluid reconstruction to correct any diluting/mixing and gas loss along the path to the ground surface. This program employs a set of objective criteria to estimate reservoir temperatures to reduce the ambiguity inherent in judging the clustering of computed $\log(Q/K)$ curves by more subjective “eyeballing.” Coupled with numerical optimization using PEST, an external parameter estimation software (Doherty 2008), GeoT can estimate unknown or inaccurate input parameters necessary to

reconstruct the deep reservoir composition (e.g., amount of fluid degassing and/or dilution).

GeoT was developed based on existing methods and routines, including TOUGHREACT (Xu et al. 2011), SOLVEQ/CHILLER (Reed 1982, 1998) and GEOCAL (Spycher and Reed, unpublished). The core of the software is a homogeneous geochemical speciation algorithm, solving mass balance/mass action equations by Newton–Raphson iterations. The saturation indices of minerals ($\log(Q/K)$) are calculated using the ion activity product (Q) and the thermodynamic equilibrium constant (K). An external thermodynamic database is necessary for the calculation of activity coefficients and equilibrium constants. After entering initial parameters, the program reconstructs deep fluid compositions and estimates reservoir

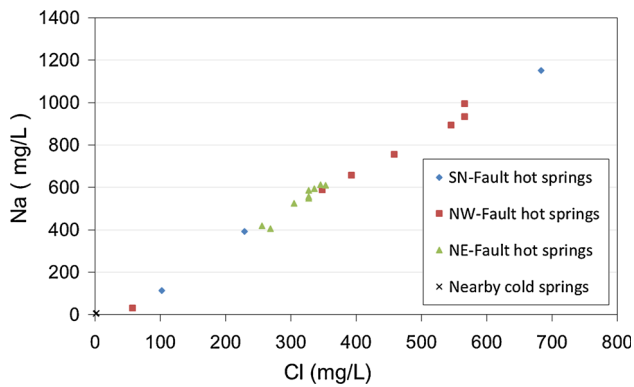


Fig. 3 Plot of Na⁺ versus Cl⁻ concentrations in Tengchong geothermal waters

temperatures by numerically assessing the clustering of computed mineral saturation indices (Spycher et al. 2013, 2014). Input parameters include specific minerals, aqueous concentrations, gas composition, initial temperature, steam fraction of discharge, etc. Here, we use the IMG method by coupling GeoT with PEST to simulate a total of 13 samples from the Tengchong field.

Results and discussion

Insights from a single spring

Previous estimation of reservoir temperatures in Tengchong

Because of limited deep drilling information, there is no accurate data about the deep reservoir temperature of the Rehai field near the Tengchong region. In the Tengchong geothermal survey of 1976, the first geothermal drilling was constructed on the south bank of the Zaochang River, which reached a depth of 26 m and yielded a temperature of 96 °C. According to the “Geothermal Survey Report of Tengchong County, Yunnan Province (1987),” the deepest borehole at the time was 400 m, and the measured temperatures in all boreholes were below 100 °C (Guo 2013). In the 1990s, the Yunnan geological survey team of The China National Nuclear Corporation drilled a 400-m deep borehole in Tengchong, which yielded a measured temperature of 142 °C at 380 m depth. In 1997, with the support of the State Science and Technology Commission, the Yunnan Geothermal Development Limited Liability Company drilled a 1640-m deep borehole near Tengchong yielding a measured bottom temperature of 150 °C (Zhang and Duan 2005). From these studies, the maximum reported borehole temperature was less than 200 °C, which is below geothermometry results reported by previous investigators using different methods. This is probably

because most of these boreholes were shallow, and the few other deep boreholes that were investigated did not reach the real geothermal reservoir (Zhang and Duan 2005). Guo (2013) used the Na–K geothermometer and Si-enthalpy graphic method to estimate the reservoir temperature, and obtained a temperature of 250 °C. Using a variety of classical geothermometers and considerable chemical data, Tong and Zhang (1989) obtained an average value of 215 ± 28 °C. Integrating Na–K geothermometer, SiO₂ geothermometer and carbon isotope geothermometer data, Shanguan (2000) derived a temperature range of 250 ± 7 °C. Synthesizing the results of previous investigations, the range of 200–250 °C could be a reasonable temperature range in the Rehai geothermal field near the Tengchong volcanic region.

Initial analysis of sample RH01

Because RH01 (Dagunguo Hot Spring) is the largest flow and temperature geothermal spring of the area, it was chosen for further investigation. Due to the lack of dissolved Al concentration data, we started our analyses with an approximate value of 0.05 mg/L previously estimated by Zhang et al. (2004). Because the Mg concentration is below the detection limit, we initially take the Mg concentration as the minimum detectable value (0.01 mg/L). In this first (base) case, without parameter optimization and deep fluid reconstruction, the calculated mineral saturation indices (SI) show poor clustering as a function of temperature, with a GeoT estimated temperature around 208 °C (Fig. 4a). This program computes various statistical functions of saturation index values that can be used to formulate objective functions for numerical optimization. These include the median (RMED), mean root square error (RMSE), standard deviation (SDEV) and average (MEAN) of absolute SI values (Fig. 4b). The reservoir temperature is taken as the temperature at which the RMED value is minimal (Spycher et al. 2014). As shown in Fig. 4b, the computed RMED in the base case is high (0.46), and the other statistical functions depart significantly from zero, indicating poor performance of the geothermometry approach without deep fluid reconstruction. Temperatures estimated with classical geothermometers are also shown in Fig. 4b; all are higher than 280 °C, significantly higher than values expected from previous investigations.

Fix-Al method

Among the selected nine major minerals (see “Mineral assemblage and thermodynamic data” section), six are aluminosilicate minerals: albite-low, montmorillonite-ca, microcline, laumontite, muscovite and clinocllore. The Al concentration of geothermal fluids is an important factor

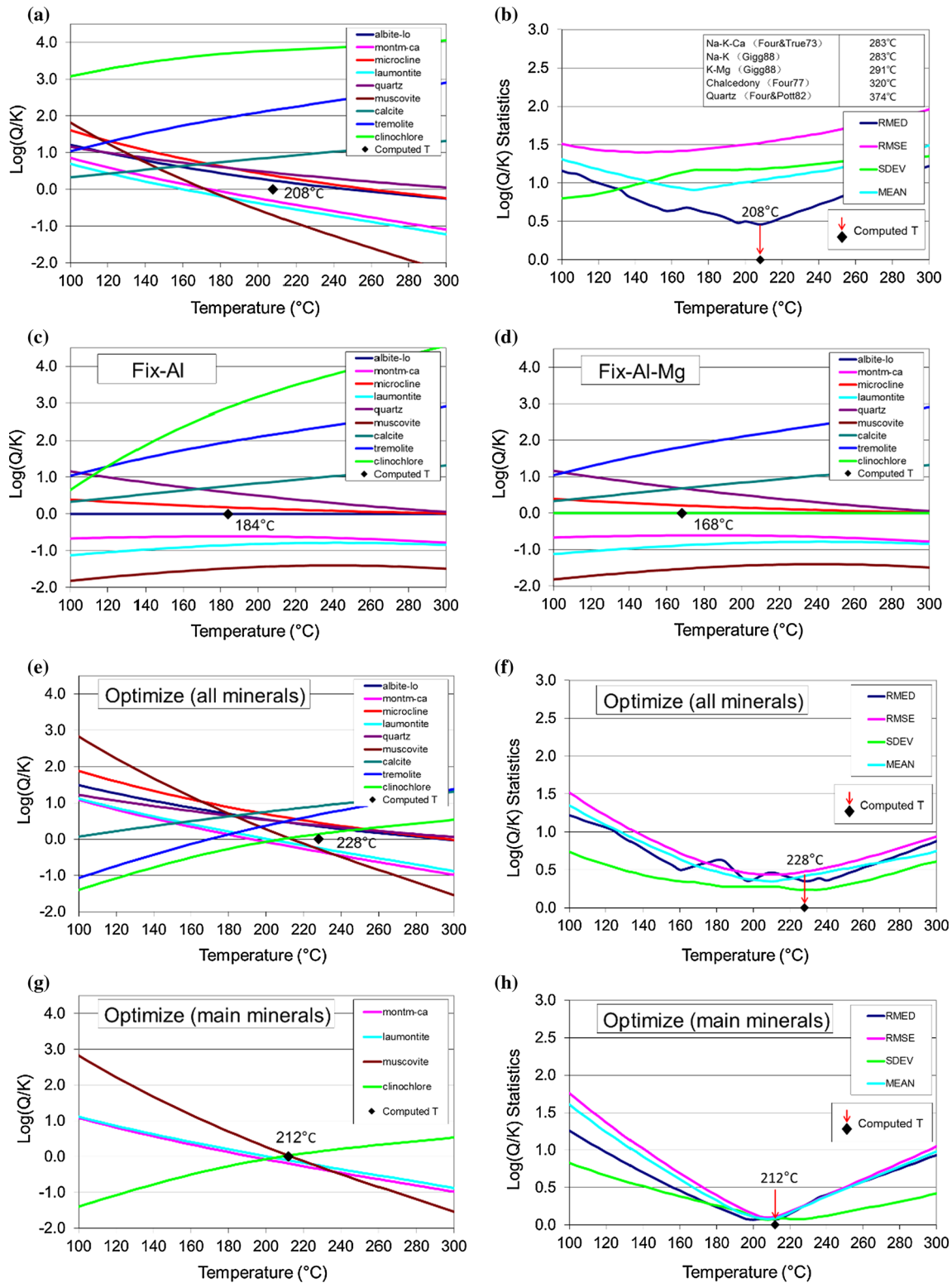


Fig. 4 Simulation results of Dagunguo geothermal spring obtained by the integrated multicomponent geothermometry method. **a** Mineral saturation index variation with temperature for the base case. **b** Statistical analysis for the base case (including the results of classical geothermometers). **c** Mineral saturation index variation with temperature for the Fix-Al case. **d** Mineral saturation index variation with temperature for the Fix-Al-Mg case. **e** Mineral saturation index

variation with temperature for the case of numerical optimization. **f** Statistical analysis for the case of numerical optimization. **g** Mineral saturation index variation with temperature for the numerical optimization (considering the major minerals). **h** Statistical analysis for the case of numerical optimization (considering the major minerals)

for determining the Al-containing mineral equilibrium assemblage (Pang and Reed 1998). However, Al concentration is often missing or inaccurate. Pang and Reed (2010) pointed out that the error in Al data will affect the determination of the original mineral equilibrium. If we decrease the Al concentration, all $\log(Q/K)$ curves of the Al-containing minerals will move to the unsaturated field, while other minerals do not change. Thus, the Al concentration should be corrected before applying the IMG method. For the same reason, the concentration of Mg should also be corrected.

The Mg concentration controls the equilibrium of clinocllore. In the case above, since Mg was not detected in this sample, we took the detection limit (0.01 mg/L) as input of the Mg concentration. When doing so, the value of the clinocllore saturation index is greater than 3 over the entire temperature range, which shows that the Mg detection limit (0.01 mg/L) is likely much greater than the actual concentration. Reducing the input of Mg concentration will improve the $\log(Q/K)$ curve of clinocllore (not shown). Therefore, the Mg concentration should also be corrected like the Al concentration.

If minerals in a geothermal system contain common components, their equilibrium is interdependent. When the Al concentration is inaccurate or unknown, we can assume that aqueous Al is fixed to a particular Al-containing mineral at different temperatures, and we can then use the obtained Al concentration to calculate the $\log(Q/K)$ value of other Al-containing minerals. This method was named the Fix-Al method by Pang and Reed (1998), and it works well for most geothermal systems containing at least two Al-containing minerals. The same approach can also be applied to the Mg concentration. Forcing the Al concentration to yield equilibrium with albite-low, the resulting temperature is 184 °C (Fig. 4c); however, the saturation index curves do not show good clustering at any specific temperature. If we apply the Fix-Al method in addition to forcing the Mg concentration to yield equilibrium with clinocllore, the result is 168 °C (Fig. 4d), which still producing poor clustering of the saturation index curves. These results show that the Fix-Al method is not effective in this case.

Numerical optimization

The GeoT program can be coupled with external numerical optimization software to minimize the clustering of mineral saturation indices by estimating some of the unknown or poorly constrained input parameters. In this case, PEST (Doherty 2008) was used to estimate by numerical optimization: the Al and Mg concentrations; the dilution/concentration factor (“cfact,” representing dilution when its value is >1); and also the steam fraction (“sf,” the fraction

of gas in the total discharge). The following average gas composition was estimated from analyses of gas samples in geothermal wells (Shangguan et al. 2000) to reconstitute the “pre-boiled” fluid composition: 99.86 mol% H₂O (wet gas) and 95.41 mol% CO₂, 0.43 mol% H₂, 0.023 mol% H₂S, 0.01 mol% CH₄ (dry gas).

The steam fraction was used to add back into the deep fluid composition the steam lost by boiling. The major “dry” gas in this case is CO₂, so the steam fraction parameter was used to correct for the effect of CO₂ loss (and accompanying pH rise) on the fluid–mineral equilibria. Because sulfide minerals are not considered in this case, a very small amount of H₂S gas does not affect mineral equilibria. The dilution/concentration factor corrects for the effect of dilution with shallow water mixing or concentration with ground surface evaporation.

Using the IMG method, thus with numerical optimization with GeoT-PEST to estimate the Al and Mg concentration in the RH01 water sample, as well as the dilution factor and steam fraction, we obtain 0.23 mg/L for the Al concentration, 0.05 µg/L for the Mg concentration, a dilution factor of 1 (no dilution) and a steam fraction of 0.04 (Fig. 4e, f). In this case, the clustering obviously improves, although a wide range of values still exist (Fig. 4f), yielding an estimated reservoir temperature of 228 °C. It is not difficult to see that a large spread of temperatures (over 100 °C) is indicated by the $\log(Q/K)$ curves of minerals crossing the equilibrium point (zero $\log(Q/K)$ values), which shows that these minerals may not all be near equilibrium with the reservoir fluid. Considering only a subset of best-clustering minerals (montmorillonite-ca, laumontite, muscovite, clinocllore) yields a temperature of 212 °C (Fig. 4g, h), and the spread of results computed with these four minerals is less than 20 °C; thus, it is better constrained than the previously estimated temperature. In this case, the numerical optimization, together with fluid reconstruction, yields a temperature that is more in line with results from previous investigations.

Reservoir temperature estimations

Heat sources and rising path of the geothermal fluid

In addition to Sample RH01, other spring samples in Rehai geothermal field were investigated using the IMG method (Table 2). In these cases, the same minerals were used as in the previous analyses: quartz, albite, microcline, clinocllore, muscovite, calcite, tremolite, laumontite and montmorillonite-Ca. We divided the springs into three groups according to their location. Group 1 includes RH01, RH02, RH06 and RH09, which are distributed on the same fault (Fig. 1c). Group 2 includes RH03, RH04, RH05, RH07 and RH08, which are distributed on another fault

Table 2 Temperatures calculated from classical geothermometers and integrated multicomponent geothermometry, and values of parameters estimated by numerical optimization, cfact, concentration/dilution factor; sf, steam fraction, Al concentration (mg/L) and Mg concentration ($\mu\text{g/L}$)

Sample no.	pH	Using original composition				Using reconstituted composition				T_{geoT}	T_{stdev}	Optimized parameters			
		T_{quartz}	$T_{\text{Na-K}}$	$T_{\text{Na-K-Ca}}$	$T_{\text{K-Mg}}$	T_{quartz}	$T_{\text{Na-K}}$	$T_{\text{Na-K-Ca}}$	$T_{\text{K-Mg}}$			Al	Mg	cfact	sf
RH01	8.3	311	283	283	–	359	283	283	523	212	9	0.23	0.05	1.00	0.04
RH02	6.8	224	300	271	–	210	300	269	308	212	10	0.19	0.90	0.90	0.08
RH03	6.4	199	311	236	121	221	311	239	235	250	6	0.80	1.60	1.30	0.00
RH04	8.9	282	288	278	–	238	288	271	370	250	9	0.35	0.50	1.00	0.39
RH05	8.9	282	282	289	–	251	283	284	382	246	12	0.32	0.26	1.00	0.31
RH06	2.6	214	630	315	115	238	631	319	119	216	66	2.70	1300	1.30	0.00
RH07	8.4	210	284	272	215	209	284	272	381	224	6	0.28	0.50	1.20	0.20
RH08	7.6	251	283	263	–	227	283	259	378	240	8	0.42	0.22	0.83	0.11
RH09	7.5	199	338	245	124	194	338	244	322	206	9	0.42	0.27	1.00	0.08
RH10	9.2	266	287	270	179	219	287	263	306	234	9	0.40	1.20	1.00	0.43
RH11	6.9	217	270	244	188	209	270	242	329	228	5	0.40	0.50	1.00	0.11
RH12	8.2	222	267	242	173	214	267	240	332	230	4	0.34	0.45	1.11	0.20
RH13	8.3	204	286	250	167	204	286	249	358	224	6	0.35	0.45	1.20	0.18

Temperature is in degrees Celsius. T_{stdev} is the standard deviation of these temperatures

(Fig. 1c). Group 3 includes RH10, RH11, RH12 and RH13, which are located along the Zaochang River (Fig. 1c).

Group 1 yields similar temperatures (212, 212, 216, 206 °C), which indicates that these springs probably share a common fracture path. Group 2 also yields similar but higher temperatures (250, 250, 246, 240 °C), except for RH07 (224 °C), suggesting that these springs may have a common fracture path. Group 3 also presented similar temperatures (234, 228, 230 and 224 °C), indicating that these springs likely have the same fracture path as well. In particular, Group 3 is located on Fault 38 while Group 2 is located at the intersection of Fault 38 and an accompanying fault, and the two groups are also close to the Zaochang River (Fig. 1c). In these structural conditions, the estimated temperature of RH07 (Group 2) is in the range of Group 3 temperatures (224–234 °C) and the two groups yield similar reservoir temperatures. Thus, we infer that Group 2 and Group 3 might have a common rising path and are differentiated only by mixing with different shallow waters.

Optimized parameters

As can be seen from Table 2, most of the water samples are affected by gas loss, which removes CO_2 and other gases from the solution, resulting in a pH rise. RH04, RH05 and RH10 have higher pH values (8.9, 8.9, 9.2), mainly because of the loss of CO_2 ; thus, adding gas back to the solution to reconstruct the original fluid is important. Simulation results confirm this assumption of gas loss, as these three samples yield the highest steam fraction values (0.39, 0.31 and 0.43).

In Group 1, RH01, RH02 and RH09 yield less gas loss, with computed steam fractions of 0.04, 0.08 and 0.08, respectively. The concentration factor of RH06 is 1.30, which adjusts for dilution. On the contrary, the computed concentration factor for RH02 is less than 1 (0.9), thus correcting for an evaporative concentration effect.

In Group 2 (RH03–08), all the springs except for RH03 have nonzero steam fractions (0.39, 0.31, 0.20 and 0.11), which indicates that gas loss is a common process. RH04 and RH05 have higher steam losses, RH03 and RH07 are affected by dilution (1.30 and 1.20) and RH08 is affected by concentration (0.83).

The springs in Group 3 (RH10–13) are also affected by steam loss, with steam fractions of 0.43, 0.11, 0.20 and 0.18. Dilution factors of RH12 and RH13 are 1.11 and 1.20, respectively.

The effect of reconstituted deep fluid on classical geothermometers

As shown in Table 2, deep fluid reconstruction has an effect on the results of classical geothermometers. There is no effect on the Na–K geothermometer, because it is not affected by dilution or concentration. With this geothermometer, lower Na/K ratios yield higher temperatures. Thus, overestimated temperatures could result from K concentrations higher than those dictated by the albite/K-spar equilibrium. The Na–K–Ca geothermometer results are not significantly affected by the reconstruction either. As shown in Fig. 5, because of dilution/concentration effects, there are larger differences between the original

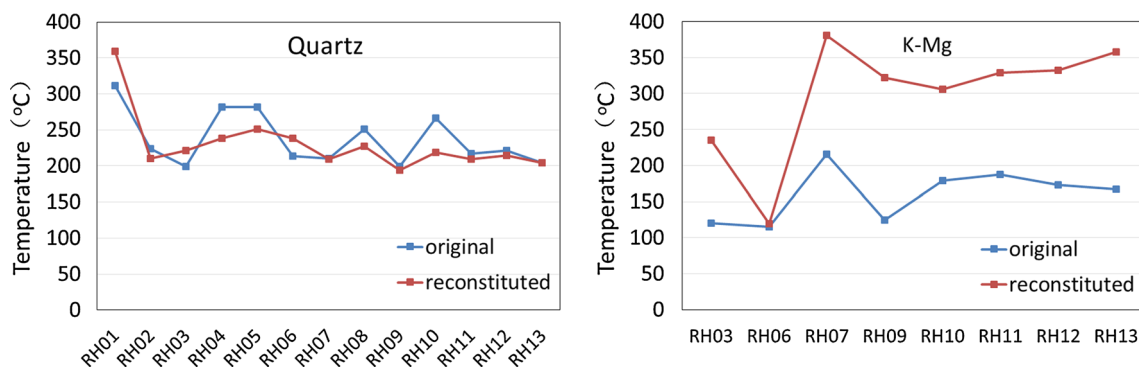


Fig. 5 Difference in calculated temperatures between reconstituted deep fluid and original deep fluid using classical geothermometers

quartz geothermometer results and those obtained using the reconstituted fluid component. The largest differences lie with the K–Mg geothermometer, because this geothermometer is a function of the square of the K concentration. The K–Mg temperatures of the reconstructed fluid are much higher than those calculated using the original fluid composition. As shown in Table 2, the measured Mg concentration of some springs (RH01, RH02, RH04, RH05 and RH08) is below the detection limit; thus, we do not report K–Mg geothermometer results using the original fluid composition for these springs (Fig. 5). Note that the purpose of the reconstituted deep fluid is to correct the clustering of minerals curves in the IMG, but it is not completely applicable for classical geothermometers.

IMG versus classical geothermometer

The comparison of the IMG simulated temperatures (GeoT) with classical geothermometer results is shown in Fig. 6. It is clear that the quartz geothermometer results are generally closest to IMG simulated temperatures. Thus, in this case, the temperatures calculated from the quartz geothermometer seem more reasonable than other classical

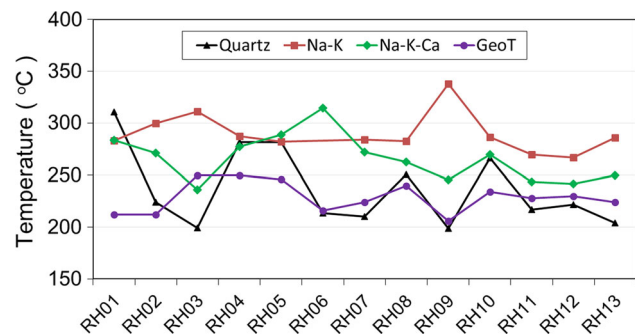


Fig. 6 Comparison of temperatures obtained from the integrated multicomponent geothermometry with those calculated by classical geothermometers (uncorrected fluid compositions) for different springs in the Tengchong geothermal field. The anomalously high Na–K value (above 600 °C) of point RH06 was excluded

geothermometers. The Na–K geothermometer results are much higher than the IMG temperatures. The results of the Na–K–Ca geothermometer, which aims to correct abnormally high Na–K temperatures, are better than those of the Na–K geothermometer, but are still apparently too high. Due to missing or inaccurate Mg concentration data, the K–Mg geothermometer results are not drawn on Fig. 6. From Table 2, the K–Mg geothermometer results are generally low, which is mainly because K–Mg solution equilibration is rapid and re-equilibration occurs when the deep fluids ascend to the ground surface (Giggenbach 1988).

Conclusion

Based on integrated multicomponent geothermometry (IMG), which couples numerical optimization with the mineral saturation index method, we have investigated geothermal reservoir temperatures for the Tengchong geothermal field in southwestern China. The main conclusions can be drawn as follows:

1. The reservoir temperatures of the Rehai geothermal field in the Tengchong volcanic region, obtained from the IMG method, range from 206 to 250 °C, with an average temperature and standard deviation of 229 ± 14 °C. Temperatures calculated from the quartz geothermometer are closest to the IMG results, which demonstrates that quartz may be a reasonable classical geothermometer for estimating reservoir temperatures of the Rehai geothermal field springs, with the exception of a few springs like RH01 and RH03.
2. The optimized Al concentrations are between 0.19 and 0.42 mg/L for all springs, with the exception of RH03 and RH06, and the optimized Mg concentrations are between 0.05 and 1.2 μg/L. Dilution and gas loss often occur when geothermal fluids ascend to the ground surface.

3. All of the hot springs have a common deep heat source, but their rising paths are controlled by the fault on which they are located. Group 2 and Group 3 might have a common rising path and are differentiated only by mixing with different shallow waters. Using the IMG method together with classical geothermometers can significantly increase confidence in reservoir temperature estimations.

Acknowledgements This work was supported by the National Natural Science Foundation of China (Grant Nos. 41572215 and 41402205) and the China Geological Survey, Geothermal Resources Investigation in Xining-Guinan of Qinghai Province (Grant Nos. 12120115046201 and 121201012000150011).

References

- Ding ZL (2013) Solid earth science research methods. Science Press, Beijing, pp 219–242
- Doherty J (2008) PEST—model-independent parameter estimation. Watermark Numerical Computing, Corinda 4075, Brisbane, Australia. <http://www.sspa.com/pest/>
- Fournier RO (1979) A revised equation for the Na/K geothermometer. Geotherm Resour Council Trans 3:221–224
- Fournier RO, Potter RW (1982) Revised and expanded silica (quartz) geothermometer. Bull Geotherm Resour Counc 11(10):3–12
- Fournier RO, Truesdell AH (1973) An empirical Na–K–Ca geothermometer for natural waters. Geochim Cosmochim Acta 37(5):1255–1275
- Giggenbach WF (1988) Geothermal solute equilibria: derivation of Na–K–Mg–Ca geothermometers. Geochim Cosmochim Acta 52(12):2749–2765
- Guo TT (2013) Characteristics and genesis of geothermal field in Rehai Tengchong. Kunming University of Science and Technology, Kunming, pp 25–79
- Lin MS, Peng SB, Qiao WT, Li H (2014) Petro-geochemistry and geochronology of late Cretaceous–Eocene granites in high geothermal anomaly areas in the Tengchong block, Yunnan Province, China and their tectonic implications. Acta Petrol Sin 30(2):527–546
- Liu ML, Cao YW, Wang MD, Li JX, Guo QH (2014) Source of hydrochemical composition and formation mechanism of Rehai geothermal water in Tengchong. Saf Environ Eng 6:1–7
- Pang ZH, Reed MH (1998) Theoretical chemical thermometry on geothermal waters: problems and methods. Geochim Cosmochim Acta 62:1083–1091
- Pang ZH, Reed M (2010) Geothermometer theory and its application in geothermal research. China Geothermal energy: Achievements and Prospects—Siguang promote geothermal energy development and utilization of China 40th Anniversary Conference and China Geothermal Development Symposium
- Peiffer L, Wanner C, Spycher N, Sonnenthal E, Kennedy BM, Iovenitti J (2014) Optimized multicomponent vs. classical geothermometry: insights from modeling studies at the Dixie Valley geothermal area. Geothermics 51:154–169
- Reed MH (1982) Calculation of multicomponent chemical equilibria and reaction processes in systems involving minerals, gases and an aqueous phase. Geochim Cosmochim Acta 46:513–528
- Reed M, Spycher N (1984) Calculation of pH and mineral equilibria in hydrothermal waters with application to geothermometry and studies of boiling and dilution. Geochim Cosmochim Acta 4(7):1479–1492
- Reed MH (1998) Calculation of simultaneous chemical equilibria in aqueous mineral-gas systems and its application to modeling hydrothermal processes. In: Richards J, Larson P (eds) Techniques in hydrothermal ore deposits geology, reviews in economic geology 10:109–124
- Reed M, Palandri J (2006) SOLTHERM. H06, A database of equilibrium constants for minerals and aqueous species. Available from the authors, University of Oregon, Eugene, Oregon
- Shangguan ZG (2000) Structure of geothermal reservoirs and the temperature of mantle-derived magma hot source in the Rehai area, Tengchong. Acta Petrol Sin 16(1):83–90
- Shangguan ZG, Bai CH, Sun ML (2000) Modern mantle magma gas release characteristics of Rehai geothermal in Tengchong. Sci China 30(4):407–414
- Spycher N, Peiffer L, Sonnenthal E (2013) GeoT user's guide a computer program for multicomponent geothermometry and geochemical speciation version 1.4. Ernest Orlando Lawrence Berkeley National Laboratory, Report No. LBNL–6172E
- Spycher N, Peiffer L, Sonnenthal EL, Saldi G, Reed MH, Kennedy BM (2014) Integrated multicomponent solute geothermometry. Geothermics 51(7):113–123
- Tong W, Zhang MT (1989) Tengchong geothermal. Science Press, Beijing, pp 81–99
- Xu T, Spycher N, Sonnenthal E, Zhang G, Zheng L, Pruess K (2011) TOUGHREACT Version 2.0: a simulator for subsurface reactive transport under non-isothermal multiphase flow conditions. Comput Geosci 37:763–774
- Zhang ZX, Duan YD (2005) Tengchong of Yunnan is the best geothermal field of geothermal power development. National Symposium on Sustainable Development of geothermal industry, China
- Zhang ZS, Sun ZX, Wang SJ (2004) Successful reconstruction the equilibrium status of Tanghu hot spring by using Fixed-Al methods and its meaning. J East China Geol Inst 26(4):306–310